Check for updates

Drag on Janus Sphere in a Channel: Effect of Particle Position

Manish Dhiman
Department of Chemical Engineering,
Indian Institute of Technology Guwahati,
Guwahati, Assam 781039, India

Raghvendra Gupta[1]
Department of Chemical Engineering,
Indian Institute of Technology Guwahati,
Guwahati, Assam 781039, India
e-mail: guptar@iitg.ac.in

K. Anki Reddy
Department of Chemical Engineering,
Indian Institute of Technology Guwahati,
Guwahati, Assam 781039, India

Potential use of Janus spheres in novel engineering applications is being explored actively in recent years. Hydrodynamics around Janus spheres is different from that around homogeneous sticky or slippery spheres. Instantaneous motion of a sphere in channel flow is governed by hydrodynamic force experienced by the sphere, which in turn depends on the particle to channel size ratio, its instantaneous position, hydrophobicity of its surface, and the particle Reynolds number. We investigate numerically the drag experienced by a Janus sphere located at different off-center positions in a square channel. Two orientations of Janus sphere consisting of a sticky and a slippery hemisphere with the boundary between them parallel to the channel midplane are studied: (1) slippery hemisphere facing the channel centerline and (2) sticky hemisphere facing the channel centerline. The flow field around Janus sphere is found to be steady (for $Re \leq 50$ investigated in this work) and asymmetric. Based on the data obtained, a correlation for drag coefficient as a function of particle Reynolds number and dimensionless particle position is also proposed. [DOI: 10.1115/1.4048928]

Keywords: Janus particle, square channel, drag coefficient, CFD, off-center

1 Introduction

Janus spheres are typically the particles which have hydrophobic as well as hydrophilic properties on its surface. These are named Janus after the Roman God having two faces [1]. Recently, these amphiphilic Janus spheres having both stick and slip boundary conditions on their two hemispheres have found applications as water repellent fibers in textile industry [2], switchable screens [3], and as self-propelling particles [4]. They are also used as stabilizers in Pickering emulsions for use in food and pharmaceutical industries [5]. The above-mentioned applications involve the hydrodynamics of Janus sphere in Stokes flow while there are also instances where understanding the hydrodynamics around such particles, at high Reynolds numbers is required. For example, the problem of drag reduction over bodies using hydrophobic or hydrophilic surfaces is studied in internal [6] as well as external flows [7–9].

The forces on Janus particles of the size of nanometer in a fluid stream were investigated using molecular dynamics by Safaei et al. [10]. They varied the orientation of the Janus sphere and suggested that the forces are function of orientation of the Janus sphere. Das et al. [11] observed self-propulsion of Janus sphere experimentally. They found that the Janus particles when moving in close proximity to a solid surface exhibited an arbitrary trajectory. The "self-motile" behavior of Janus particle is also observed when the chemical composition of the solution in which the particles are immersed is altered [12]. Recently, the quantification of forces and torques on different aspect ratios of rigid Janus particles and Janus droplets in a uniform flow field is studied [13,14]. The low Reynolds number hydrodynamics for a slip-stick sphere in a uniform as well as linear shear flow is investigated by Swan and Khair [15]. They suggested that the particle migrates parallel to the velocity gradient in a linear shear flow. Trofa et al. [16] predicted the trajectories of Janus particle by varying the position, orientation, slip parameter, and confinement ratio in a cylindrical microchannel. They observed two regimes: periodic oscillation for particle positioned far from the centerline and migration towards the tube axis for those near the centerline.

The brief review suggests that there is no study in the literature that investigates the drag on the Janus particles in a low to medium Reynolds number. Therefore, in our previous work [17], we investigated the flow field and drag over Janus sphere having sticky and slippery hemispheres placed at the centerline of a square channel. The effect of particle to channel size ratio (a/H) is explored, and it is observed that drag force on Janus sphere reduces when compared to that for stick sphere. We employ free-slip and no-slip boundary conditions on the slippery and sticky surfaces of the Janus sphere, respectively.

Therefore, the effect of wall on the hydrodynamics around off-centered Janus particles is investigated in this study. The remainder of this paper is organized as follows: In Sec. 2, we present the formulation of the problem. Section 3 describes the governing equations, boundary conditions and numerical schemes to solve the system of equations. In Sec. 4, we present the pressure and velocity distribution on and around the Janus sphere, and drag experienced by it. The drag coefficient obtained for Janus sphere is compared with that for no-slip homogeneous sphere and free-slip homogeneous sphere. Based on the data obtained from computational fluid dynamics (CFD) simulations, a correlation is proposed for the drag coefficient. Finally, in Sec. 5 we state our conclusions.

2 Problem Definition

Computational fluid dynamics simulations are performed in a channel of square cross section (yz plane) of side H as shown in Fig. 1. The Janus sphere of diameter a remains fixed in the channel and the liquid flows along positive x-direction. The Janus sphere is located at a distance Y from the channel centerline on the xy plane located in the middle of the channel for all the cases. The sphere is located sufficiently away from the inlet boundary so that the flow becomes fully-developed before it reaches the sphere. The length of the channel is $L = 400a$.

[1]Corresponding author.

Contributed by the Fluids Engineering Division of ASME for publication in the Journal of Fluids Engineering. Manuscript received April 27, 2020; final manuscript received October 15, 2020; published online November 20, 2020. Assoc. Editor: Shawn Aram.

 Copyright © 2021 by ASME

Downloaded from http://asmedigitalcollection.asme.org/fluidsengineering/article-pdf/143/3/031302/6596983/fe_143_03_031302.pdf by Indian Institute Of Tech- Guwahati user on 03 August 2023

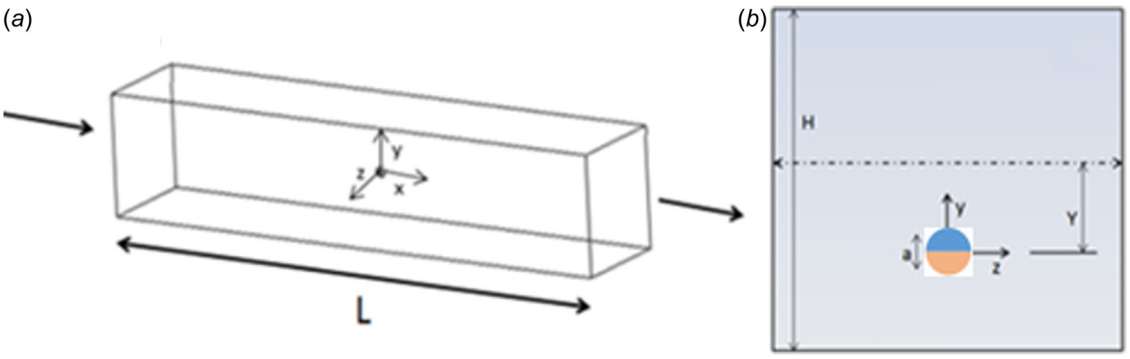

Fig. 1 (*a*) The geometric configuration of the computational domain. The origin is at the center of the sphere. (*b*) Position of Janus particle in a square (*yz*) cross section of side *H*.

The particle Reynolds number is defined as $\mathrm{Re_P} = a\rho V/\mu$. The Janus sphere considered has sticky and slippery hemispheres as shown in Fig. 1(*b*) and the boundary between the two hemispheres is on a *xz* plane. Two orientations of Janus sphere are possible-case 1: free-slip hemisphere faces the channel centerline and case 2: no-slip hemisphere faces the channel centerline.

3 Computational Methodology

Steady, laminar, incompressible, and isothermal flow is considered for a Newtonian fluid. This type of flow can be modeled by considering mass and momentum conservation equations given by Eqs. (1) and (2), respectively.

Continuity equation:

$$\nabla.\boldsymbol{v} = 0 \tag{1}$$

Momentum conservation equation:

$$\rho\left(\frac{\partial \boldsymbol{v}}{\partial t} + (\mathbf{v}.\nabla)\boldsymbol{v}\right) = -\nabla P + \mu(\nabla^2\boldsymbol{v}) \tag{2}$$

Where ρ, $\boldsymbol{v}$, μ, P, t are the density, velocity vector, dynamic viscosity, pressure, and time, respectively.

At the inlet, a uniform velocity equal to the mean fluid velocity having direction normal to inlet boundary is specified. However, the distance between channel inlet and the sphere is kept sufficient so that the flow becomes fully-developed in the channel as it approaches the sphere. At the outlet boundary, a uniform pressure (gauge pressure = 0 Pa) is specified. At the channel walls, no-slip boundary condition is specified. No-slip and free-slip boundary conditions are applied on the sticky and slippery hemispheres, respectively.

The total force acting on the sphere is calculated by integrating the pressure and viscous stresses on the sphere surface as given by Eq. 3.

$$\boldsymbol{F} = -\int_A \hat{\boldsymbol{n}} P_{\mathrm{stat}}\, dA + \int_A \hat{\boldsymbol{n}}.(\boldsymbol{\sigma} + \boldsymbol{\tau})\, dA \tag{3}$$

where $\hat{\boldsymbol{n}}$ the unit normal to the surface in the fluid, P_{stat} is static pressure, $\boldsymbol{\sigma}$ is the viscous normal stress and $\boldsymbol{\tau}$ is the viscous shear stress. Note that in this work, the symbol P denotes the total normal stress, i.e., combination of pressure and viscous normal stresses. The viscous normal stress on the wall is often negligible but can be significant on a free-slip surface. For example, for Stokes flow around a sphere having free-slip boundary condition on its surface, two-third of drag is caused by viscous normal stress and one-third is caused by pressure [18].

The drag and lift forces are calculated as components of the force along the flow direction (x) and in the direction normal to it (y).

$$F_{\mathrm{D}} = \hat{\boldsymbol{i}}.\boldsymbol{F}; \quad F_{\mathrm{L}} = \hat{\boldsymbol{j}}.\boldsymbol{F} \tag{4}$$

The drag and lift coefficients are then calculated by normalizing the drag and lift forces per unit projected area $\mathrm{A} = \left(\frac{\pi}{4}a^2\right)$ times the dynamic pressure as given by Eq. (5).

$$C_{\mathrm{D}} = \frac{F_{\mathrm{D}}}{\left(\frac{1}{2}\rho V^2\right)A}; \quad C_{\mathrm{L}} = \frac{F_{\mathrm{L}}}{\left(\frac{1}{2}\rho V^2\right)A} \tag{5}$$

The governing equations are solved using ANSYS FLUENT 19.2 [19], a finite volume based CFD software package. Second order upwind scheme [20] is used for the discretization of the convective term in the momentum equation. A pressure-based coupled scheme [21] is employed for the pressure–velocity coupling. ANSYS FLUENT 19.2, uses a colocated scheme in which both pressure and velocity are stored at cell centers. A standard scheme [22] is used for pressure discretization to interpolate the cell center values to obtain face fluxes.

4 Grid Independence

A structured, hexahedral grid is used for the simulations. The mesh is refined near the sphere and near the wall, as can be observed from Fig. 2(*c*). The first cell height near the sphere is $a/80$ for all the Y/H cases considered. The orthogonal quality of the mesh for the case, $a/H = 0.20$ and $Y/H = 0.38$ is 0.8. The orthogonality factor is defined as the angle between connection vector of cell centers and normal vector of inner face of the control volume. The Jacobian ratio is defined as the deviation of a given element from the ideally shaped element. The minimum Jacobian ratio is 0.802. Pressure distribution for the near wall Janus sphere position ($Y/H = 0.38$) for two different mesh sizes at the highest particle Reynolds number ($\mathrm{Re_P} = 50$) is shown in Fig. 2(*a*).

Further details on the grid independence and validation with the experimental and numerical studies in the literature can be found in our other works [17,23].

5 Results and Discussion

Computational fluid dynamics simulations are performed for steady, three-dimensional flow to compute the drag force on the Janus sphere placed at different positions ($0 \le Y/H \le 0.38$) in the channel for a particle to channel size ratio of $a/H = 0.20$ in the particle Reynolds numbers range of 0.1 to 50. The range of flow parameters considered in the study is given in Table 1. The density and dynamic viscosity of the fluid (water) are taken to be 998.2 kg m^{-3} and 0.001 kg m^{-1} s^{-1}, respectively. It may be noted that the flow is observed to be steady for all the cases studied in this work. This has been verified by performing a unsteady simulation at $\mathrm{Re_P} = 50$.

Downloaded from http://asmedigitalcollection.asme.org/fluidsengineering/article-pdf/143/3/031302/6596983/fe_143_03_031302.pdf by Indian Institute Of Tech- Guwahati user on 03 August 2023

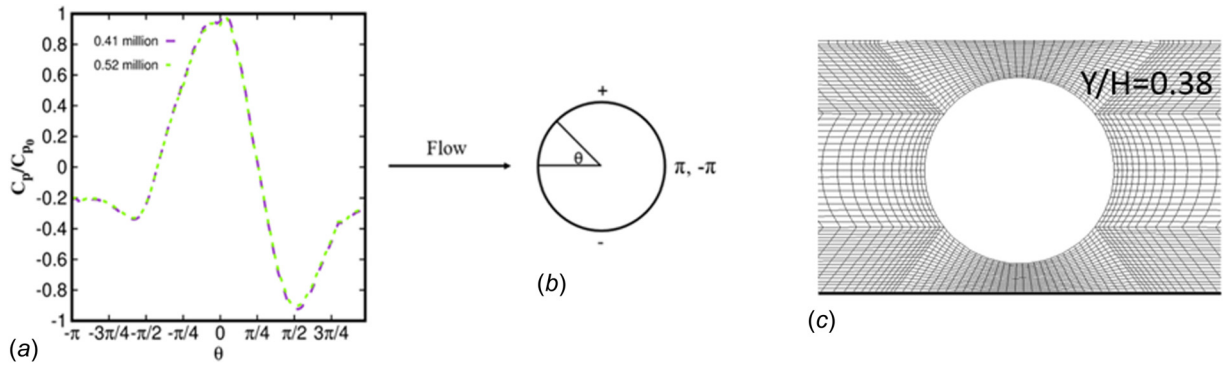

Fig. 2 (*a*) **Pressure distribution on the Janus sphere for two grid sizes. The smallest cell size next to the Janus sphere surface is *a*/80. The total number of cells between the sphere surface and the wall are 35. (*b*) The interpretation of theta (θ) on the Janus surface. (*c*) The cross section of the mesh for the Janus position near the wall (*Y*/*H* = 0.38). The dark line at the bottom represents the bottom wall.**

5.1 Pressure and Velocity Field. The contours of nondimensional pressure distribution $\left(\frac{C_p}{C_{p0}} = \frac{P-P_{\text{exit}}}{P_s-P_{\text{exit}}}\right)$ for Re_P =10 on a *xy* plane passing through the middle of the sphere are shown in Figs. 3 and 4 for cases 1 and 2, respectively. P_s is the pressure at the stagnation point at the front, P_{exit} is the pressure at the outlet. For case 1, i.e. free-slip hemisphere facing the centerline, a low pressure region exists on the free-slip hemisphere for all values of *Y*/*H*. The value of pressure is minimum for *Y*/*H* = 0.38. The pressure distribution for case 2 is different for particle locations near the centerline (*Y*/*H* = 0.10 and 0.20) than for those near the wall (*Y*/*H* = 0.30 and 0.38). While two minima in pressure exist for *Y*/*H* = 0.10 and 0.20- one each on no-slip and free-slip hemisphere, there is only one minima for the other two values of *Y*/*H*.

Table 1 The range of flow parameters studied for off-center positions of Janus sphere

a/*H*	*Y*/*H*	Re_P
0.20	0, 0.10, 0.20, 0.30, 0.38	0.1, 0.5, 1, 5, 10, 20, 30, 40, 50

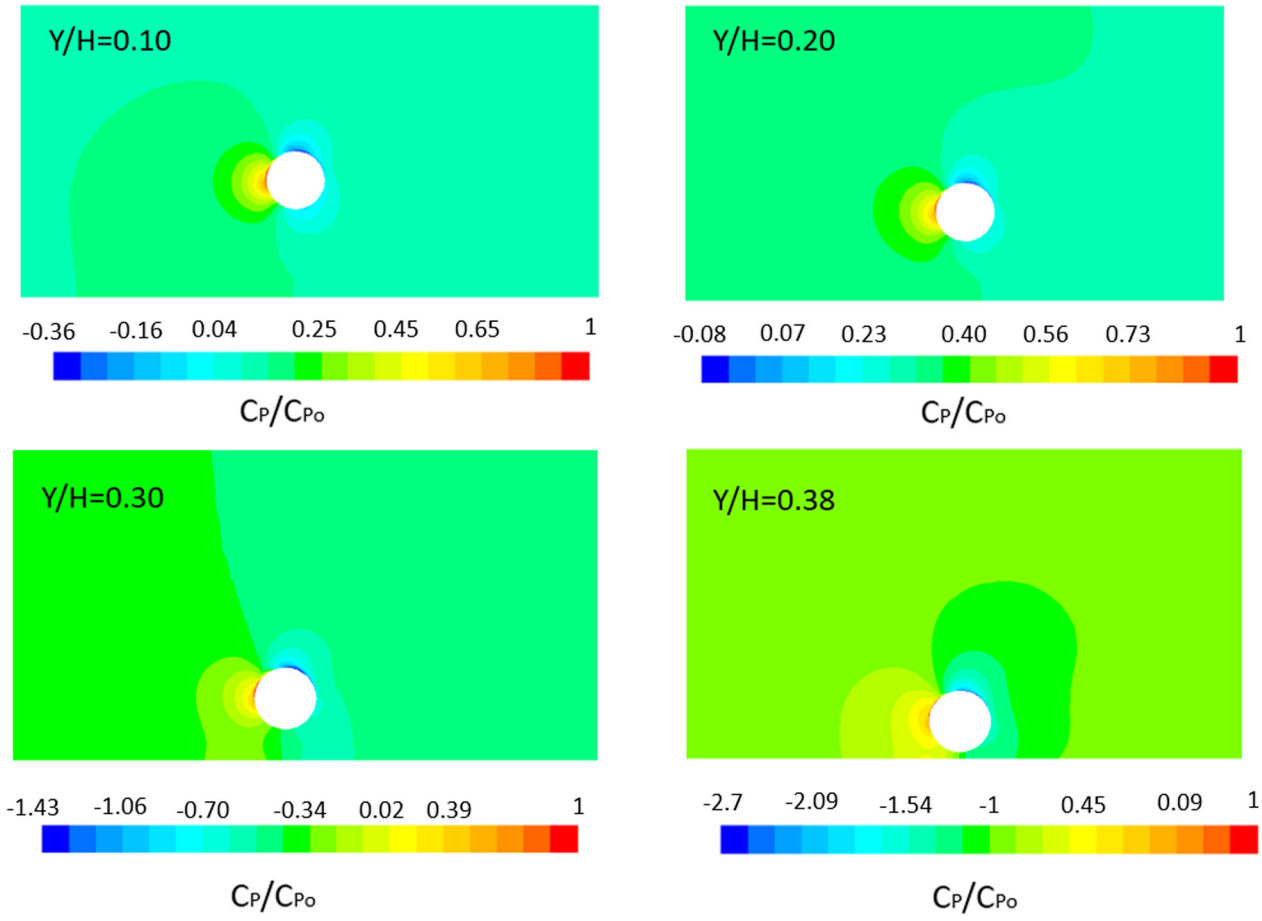

Fig. 3 Nondimensional pressure distribution $\left(\frac{C_p}{C_{p0}} = \frac{P-P_{\text{exit}}}{P_s-P_{\text{exit}}}\right)$ on the *xy* plane for *Y*/*H* = 0.10, 0.20, 0.30 and 0.38 at Re_P = 10 for case 1

Downloaded from http://asmedigitalcollection.asme.org/fluidsengineering/article-pdf/143/3/031302/6596983/fe_143_03_031302.pdf by Indian Institute Of Tech- Guwahati user on 03 August 2023

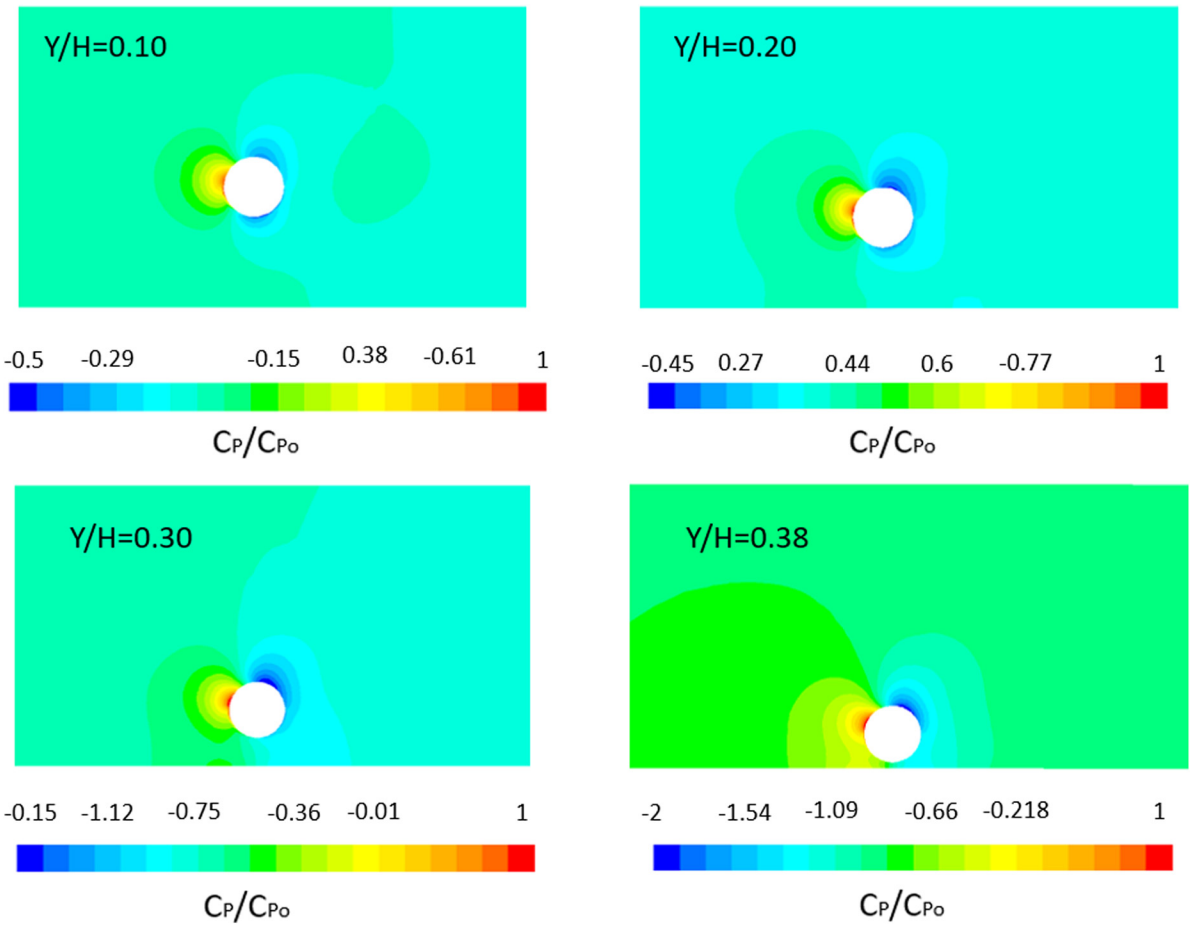

Fig. 4 Nondimensional pressure distribution $\left(\frac{C_p}{C_{p0}} = \frac{P-P_{exit}}{P_s-P_{exit}}\right)$ on the *xy* plane for *Y/H* = 0.10, 0.20, 0.30 and 0.38 at $Re_P = 10$ for case 2

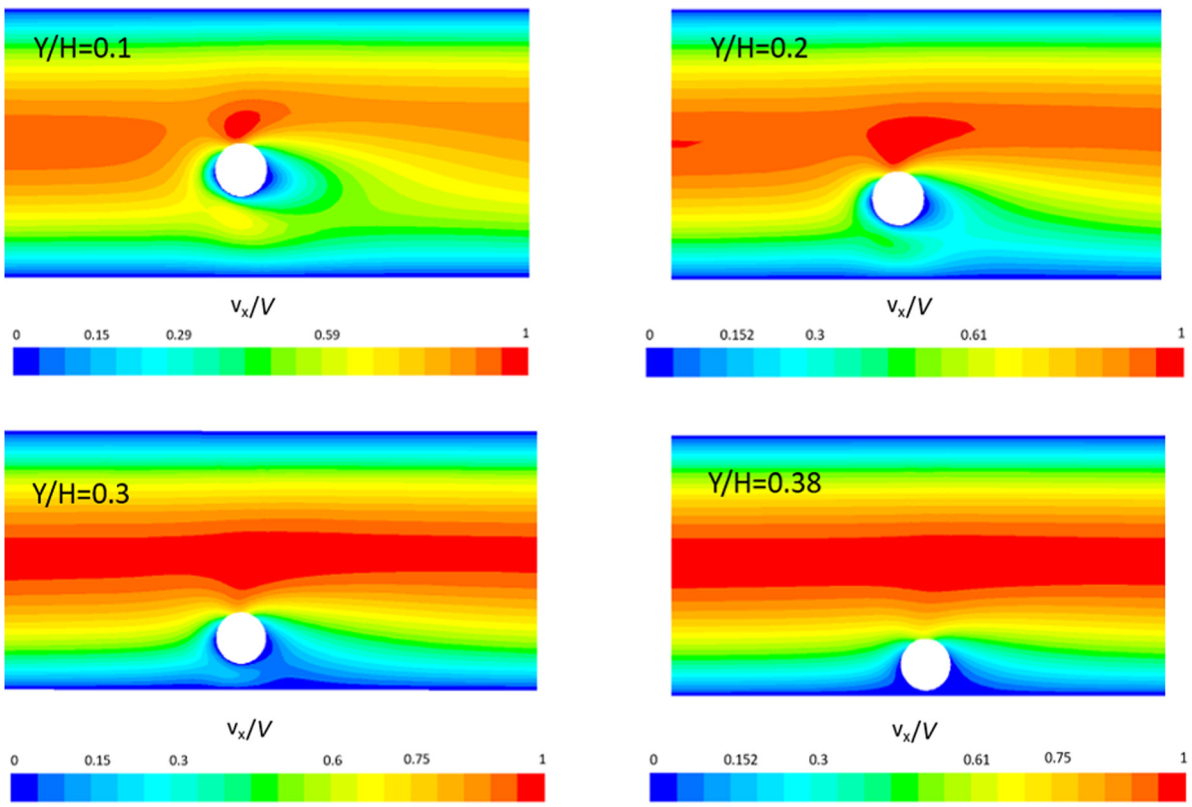

Fig. 5 *x*-velocity contours for four different locations (*Y/H*) at $Re_P = 10$ for case 1

Downloaded from http://asmedigitalcollection.asme.org/fluidsengineering/article-pdf/143/3/031302/6596983/fe_143_03_031302.pdf by Indian Institute Of Tech- Guwahati user on 03 August 2023

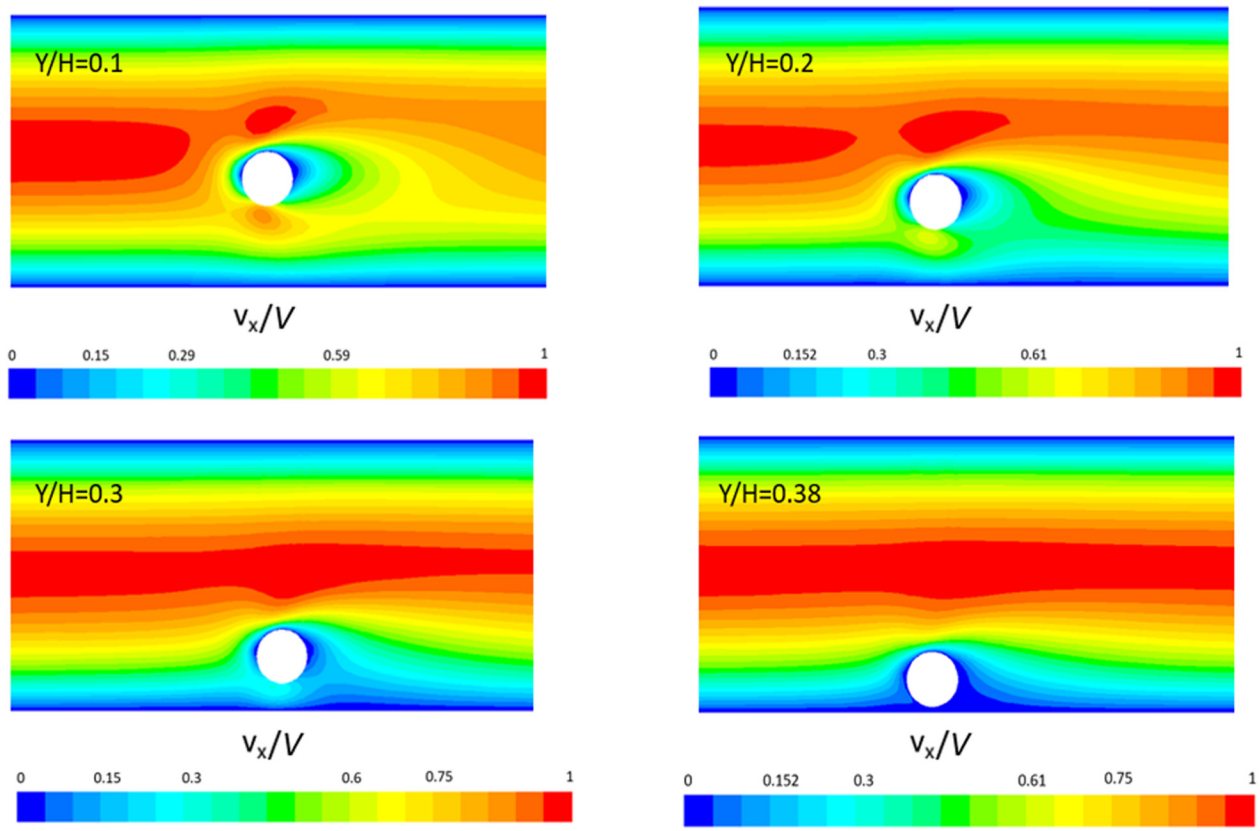

Fig. 6 ***x*-velocity contours for four different locations (*Y/H*) at $Re_P = 10$ for case 2**

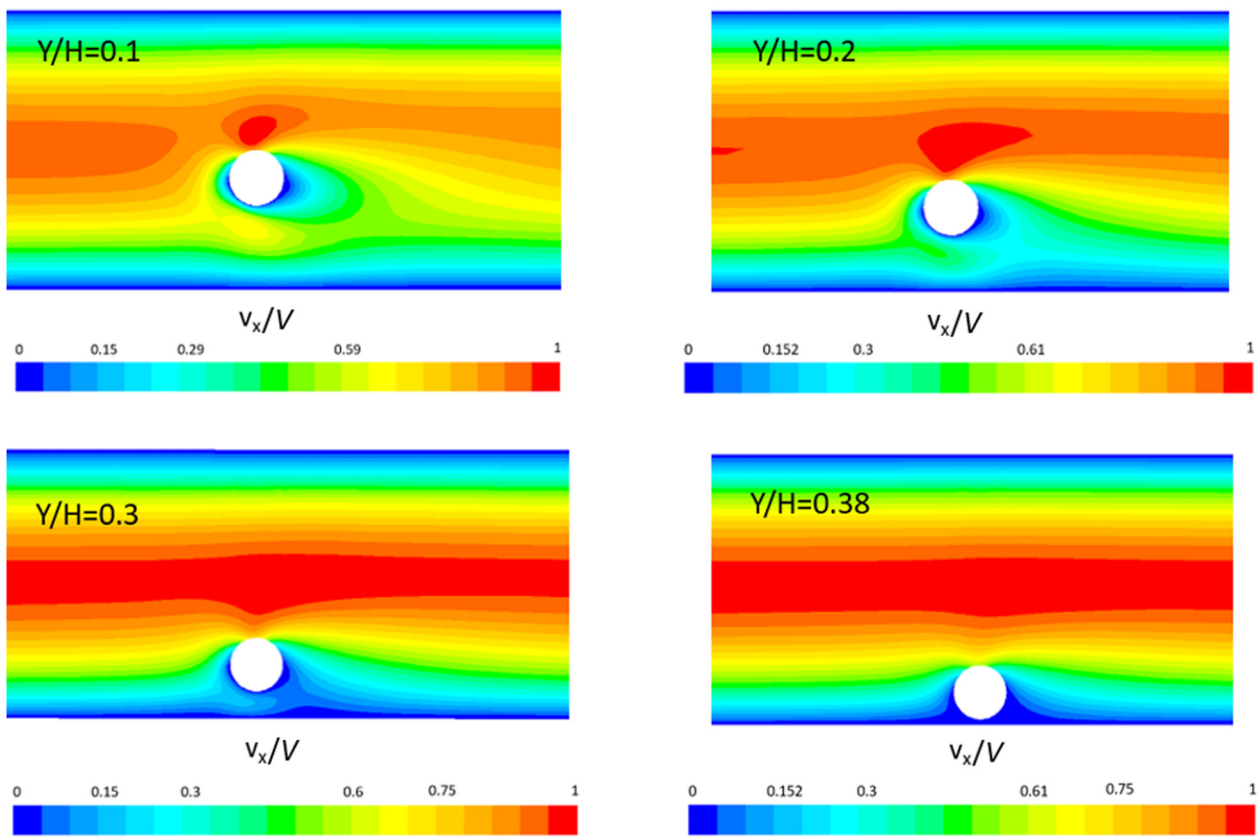

Fig. 7 ***x*-velocity contours for four different locations (*Y/H*) at $Re_P = 50$ for case 1**

Downloaded from http://asmedigitalcollection.asme.org/fluidsengineering/article-pdf/143/3/031302/6596983/fe_143_03_031302.pdf by Indian Institute Of Tech- Guwahati user on 03 August 2023

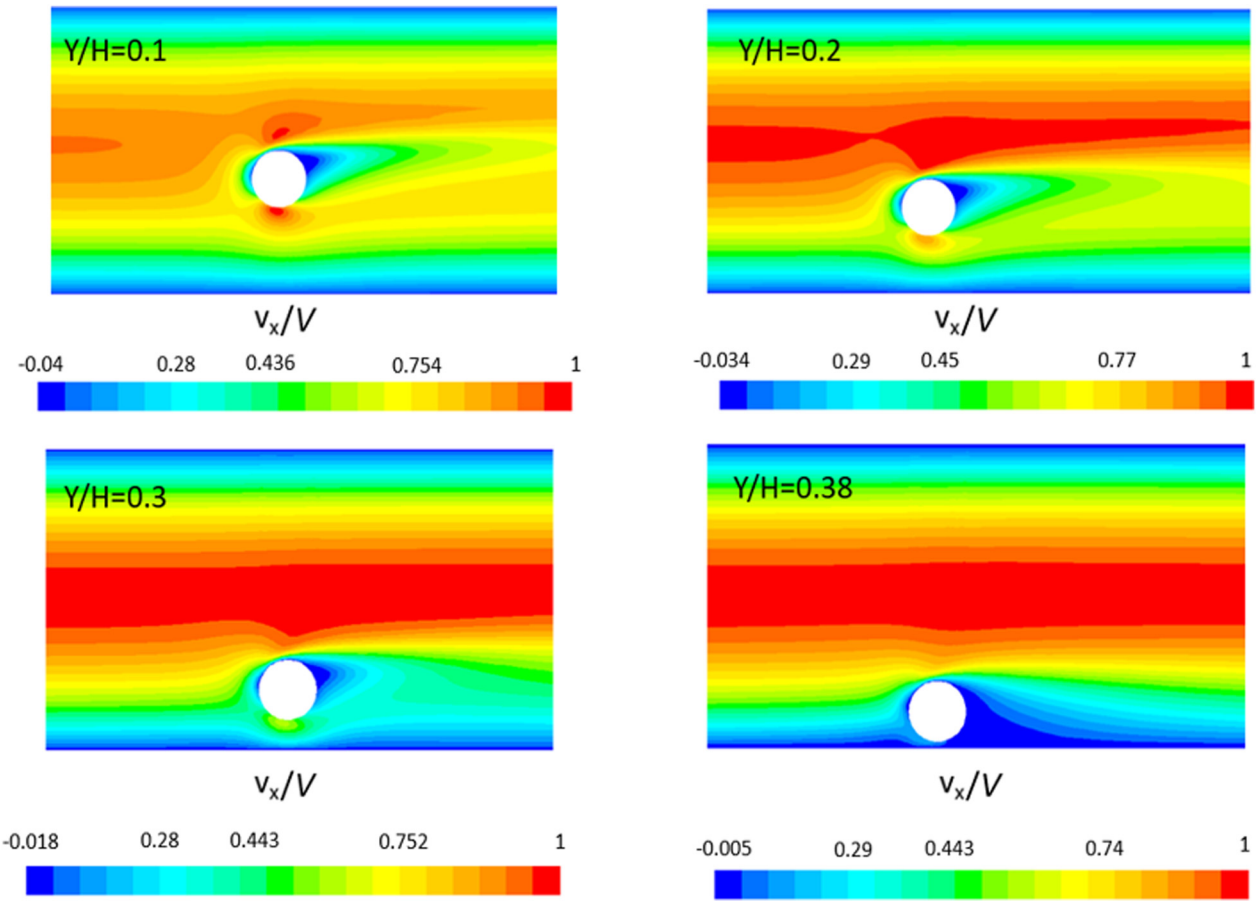

Fig. 8 *x*-velocity contours for four different locations (*Y/H*) at $Re_P = 50$ for case 2

To further understand and analyze pressure distribution on the sphere surface, velocity distribution on the same plane is plotted.

Distribution of x component of velocity in the vicinity of the Janus sphere is shown in Figs. 5–8 for different Y/H values for case 1 and 2 at $Re_P = 10$ and 50. For $Y/H = 0.1$, the surface of the sphere touches the channel centerline and affects the flow field around it on both sides of the centerline. For $Y/H = 0.2$, the sphere is close to the centerline and disturbs the flow field beyond the midplane of the channel. However, for higher values of Y/H, the velocity field on the other side of the midplane of the channel remains unaffected from the presence of the Janus sphere as is observed in our previous study for sticky spherical particles [17]. For the low particle Reynolds number ($Re_P = 10$), the flow recirculation is not observed for both the orientations of the Janus sphere as there exist only positive values of x-component of velocity in Figs. 5 and 6.

For $Re_P = 50$, a vortex is observed on the no-slip hemisphere for case 2 for all the positions of Janus particle as indicated by the negative x-component of velocity, as seen in Fig. 8. The magnitude of negative velocity and size of vortex is higher for the particle location closer to the channel centerline. However, for case 1 no flow separation is observed even at the highest Reynolds number of $Re_P = 50$. This can be attributed to the lower velocity of the fluid in the vicinity of the no-slip hemisphere in case 1.

Figure 9 shows the comparison of the x-velocity profile on the line passing through $z/H = 0.0$, for two different orientations of the Janus sphere. "1" denotes the condition when free-slip hemisphere of the Janus sphere faces the channel centerline (case 1) and "2" denotes the condition when no-slip hemisphere faces the channel centerline (case 2). It is to be noted that the velocity profile is shown for a particular position of Janus sphere in the channel ($a/H = 0.20$ and $Y/H = 0.30$ at $Re_P = 10$). There is very little effect of the presence of the sphere on the velocity in the other half of the channel. More flow passes between the wall and sphere when free-slip hemisphere faces the channel wall.

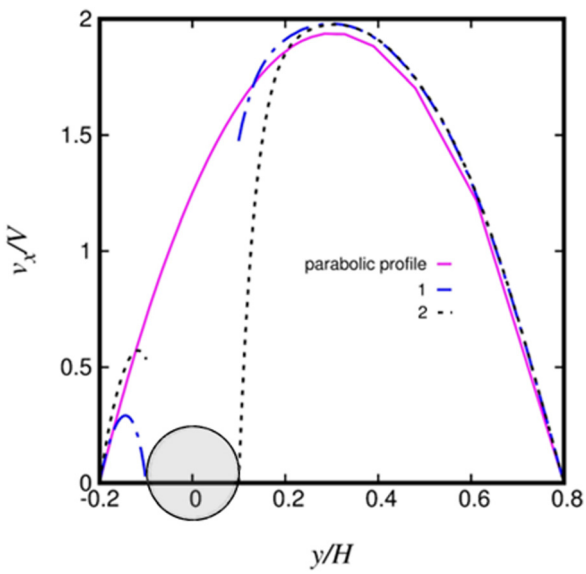

Fig. 9 Profiles of *x*-component of velocity on a line having $z/H = 0.0$ for the cross-sectional plane-upstream of the sphere for $Re_P = 10$, $a/H = 0.20$ and $Y/H = 0.30$. Here, "1" denotes the condition as in cases 1 and "2" denotes the condition as in case 2.

Downloaded from http://asmedigitalcollection.asme.org/fluidsengineering/article-pdf/143/3/031302/6596983/fe_143_03_031302.pdf by Indian Institute Of Tech- Guwahati user on 03 August 2023

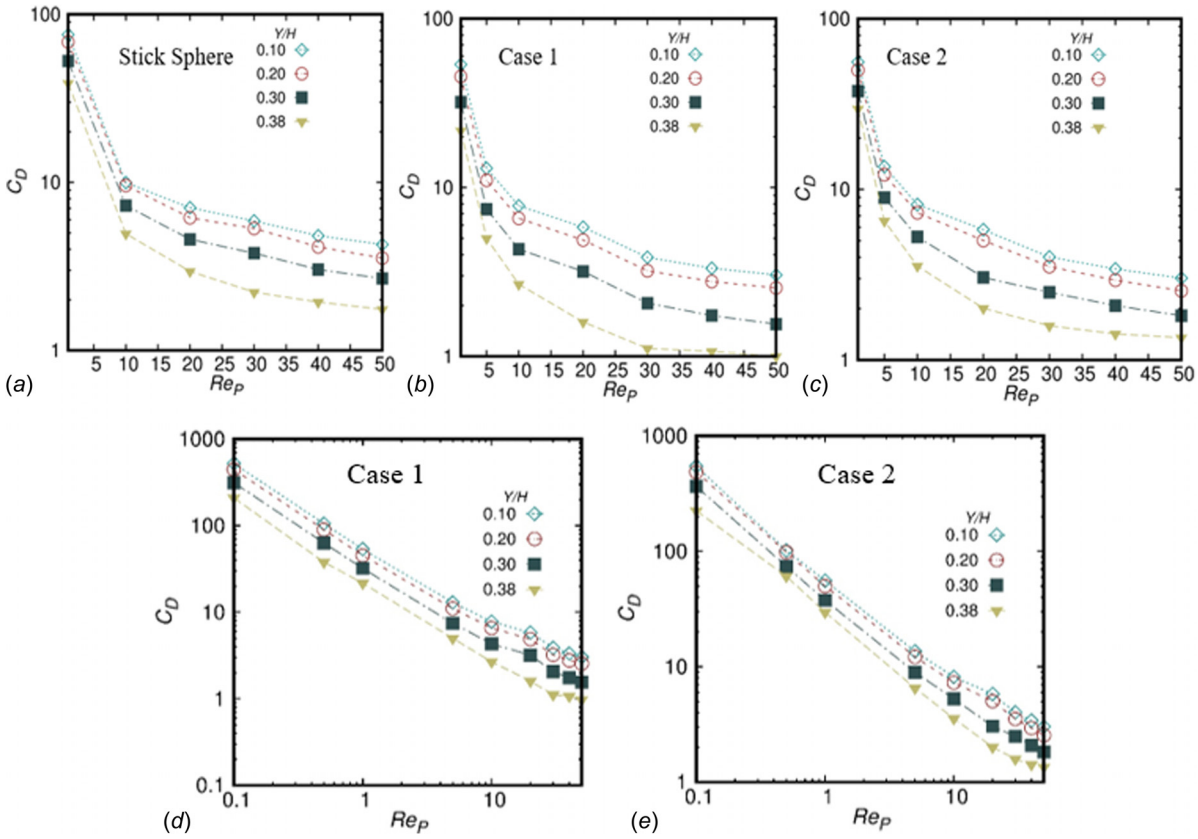

Fig. 10 Drag coefficient variation (*a*) for stick sphere (*b*) for case 1 (*c*) for case 2 (*d*, *e*) logarithmic plot for cases 1 and 2, respectively, to quantify the drag coefficient for the lowest particle Reynold numbers (0.1 and 0.5)

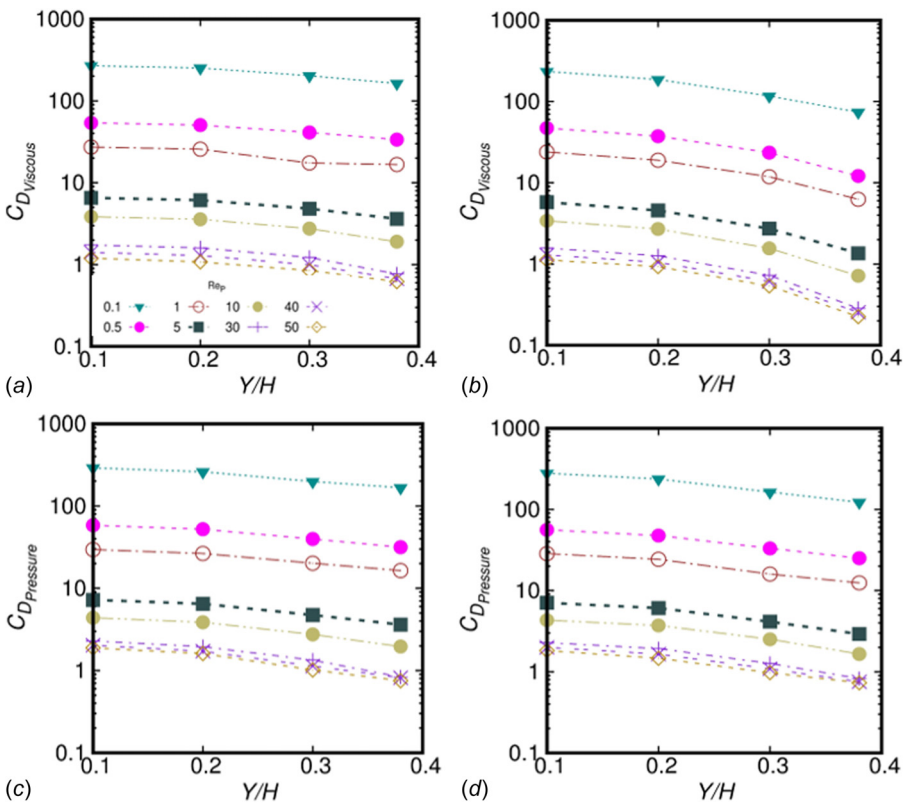

Fig. 11 Viscous and pressure contributions of drag coefficient; (*a*) and (*c*) for case 1, (*b*) and (*d*) for case 2. Symbols means the same in (*b*) (*c*) and (*d*) as in (a).

Downloaded from http://asmedigitalcollection.asme.org/fluidsengineering/article-pdf/143/3/031302/6596983/fe_143_03_031302.pdf by Indian Institute Of Tech- Guwahati user on 03 August 2023

5.2 Drag Coefficient. Drag coefficient is defined as the force per unit projected area normal to the stream wise direction nondimensionalized by the dynamic pressure $\left(\frac{1}{2}\rho V^2\right)$ for a sphere.

The variation of C_D with Re_P and Y/H is shown in Fig. 10. It is observed that the magnitude of drag coefficient for stick sphere is always the highest irrespective of its position. C_D decreases with an increase in Re_P for case 1 and 2. C_D appears to be larger for the Janus position near to the channel centerline irrespective of the orientation of the particle. However, the magnitude of C_D is higher for case 2 when top hemisphere has no-slip condition especially at high Reynolds number. The logarithmic plots for case 1 and case 2 are also shown as Figs. 10(*d*) and 10(*e*) to clearly show the drag coefficient values at low particle Reynolds numbers.

The force on the sphere is caused by the viscous and pressure contributions acting along the tangential and normal directions to the sphere surface. Figure 11 shows the contribution of viscous and pressure drags at various Y/H locations of Janus particle for various Re_P investigated. Figures 11(*a*) and 11(*b*) show $C_{Dviscous}$ as a function of Y/H for case 1 and 2, respectively. $C_{Dviscous}$ decreases as the position of Janus particle (Y/H) is varied from centerline to the wall. The higher values of $C_{Dviscous}$ is for the lowest particle Reynolds number investigated. However, the value of $C_{Dviscous}$ is lower in case 1 than that in case 2 for the same value of Y/H and Re_P. It is worthwhile to mention that the viscous drag is experienced only by the no-slip hemisphere. The trends observed for pressure components of the drag coefficient are observed to be similar (Figs. 11(*c*) and 11(*d*)) to what are observed for the viscous component with no appreciable difference between cases 1 and 2. However, it can be interpreted that the contribution of viscous force compared to that of the pressure is higher for case 2.

5.3 Local Drag Coefficient. It is well known that the drag coefficient is inversely proportional to particle Reynolds number for Stokes flow around a no-slip sphere in uniform flow. In the present case, the drag is observed to decrease significantly with an increase in Reynolds number. Therefore, the dependence of drag coefficient is presented as C_D Re_P to understand the effect of wall explicitly on the drag coefficient. Figure 12 shows the quantification of local drag coefficient and shows the increase of drag coefficient at near wall ($Y/H = 0.38$) locations.

Local drag coefficient (C_D^*) based on the velocity at the streamline approaching the center of the Janus sphere is considered. The variation of C_D^* Re_P with Re_P and Y/H is shown in Fig. 12. Note

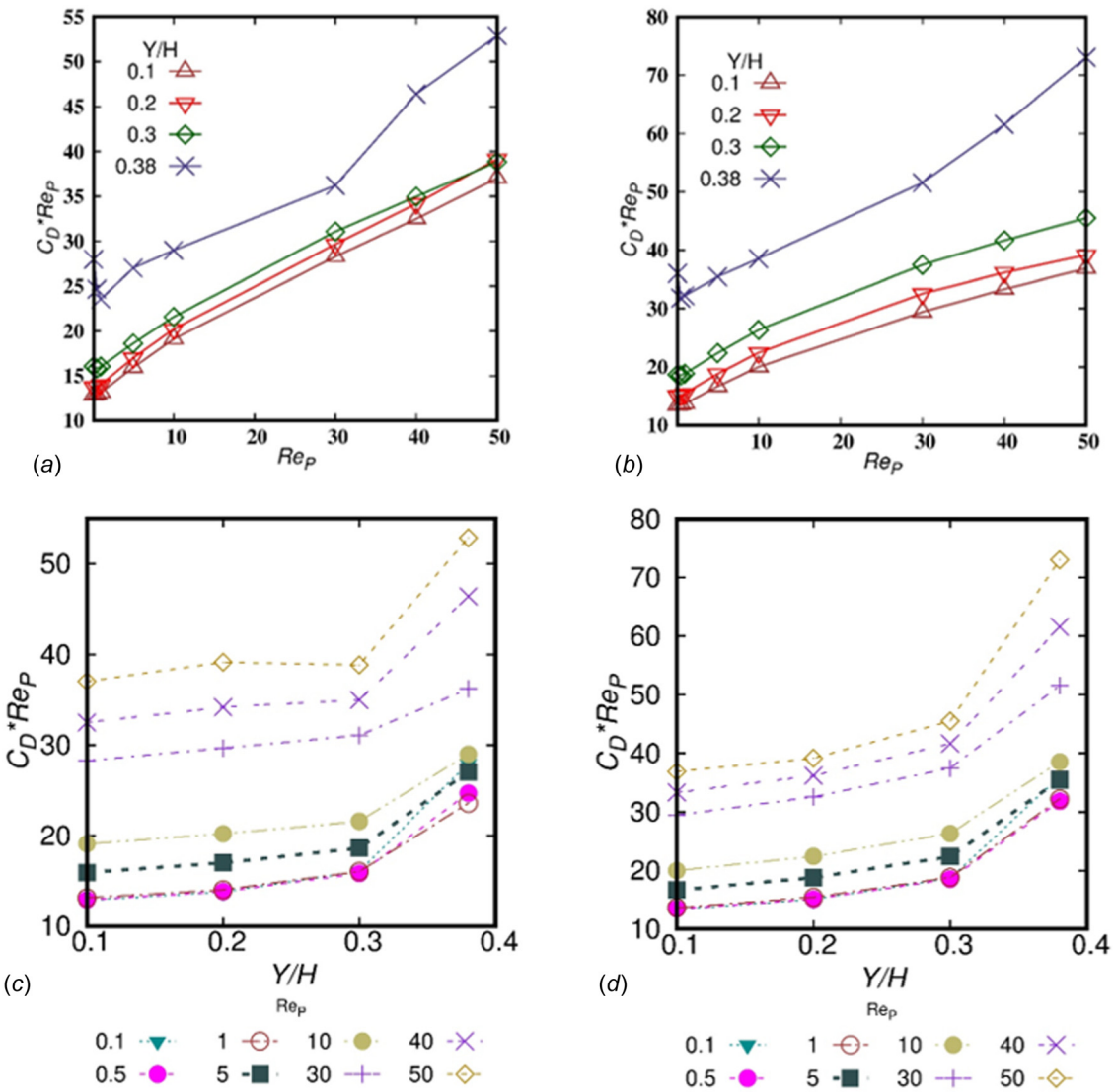

Fig. 12 Local drag coefficient variation; (*a*) and (*b*) for the orientation of Janus sphere as in case 1 and case 2, respectively, with Reynolds number and (*c*) and (*d*) with the varying Janus positions (Y/H)

Downloaded from http://asmedigitalcollection.asme.org/fluidsengineering/article-pdf/143/3/031302/6596983/fe_143_03_031302.pdf by Indian Institute Of Tech- Guwahati user on 03 August 2023

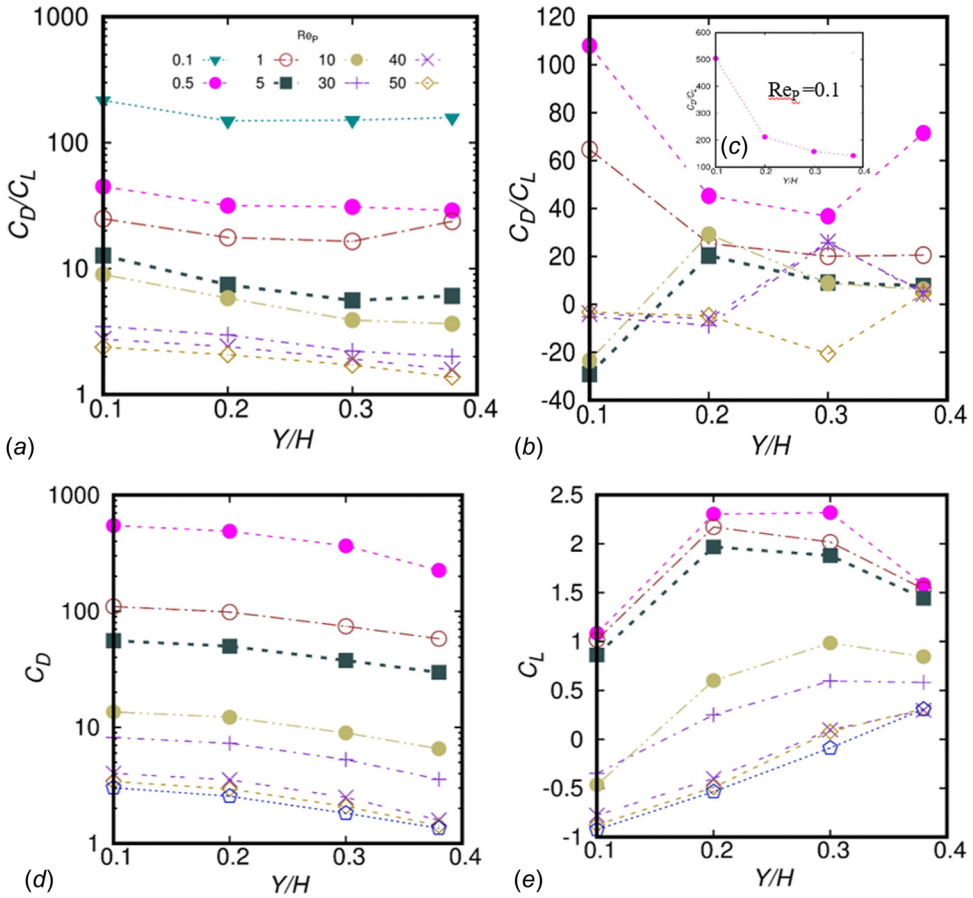

Fig. 13 C_D/C_L **at different positions of Janus sphere for (*a*) case 1 and (*b*) case 2. The inset (*c*) shows the C_D/C_L variation with *Y/H* at $Re_P = 0.1$. The drag coefficient is plotted against Janus positions in the channel for case 2. Similarly, lift coefficient variation is also shown in (*e*) for case 2. Symbols means the same in (*b*)–(*e*) as in (*a*).**

that the particle Reynolds number is based on the mean velocity in the channel. $C_D{}^* Re_P$ increases with an increase in Re_P. $C_D{}^* Re_P$ also increases with an increase in *Y/H*; a behavior opposite to that observed for C_D. This is because of the higher velocity gradient in the near wall region. There is very little effect of *Y/H* near the centerline but it sharply increases for highest value of *Y/H*. For a fixed particle Reynolds number, the local drag coefficient increases as the particle location is shifted closer to the wall. There is also a slight increase in the slope from $Y/H = 0.30$ to 0.38.

5.4 Ratio of Drag Coefficient to Lift Coefficient. The nonsymmetric flow field around the Janus sphere and offcenter location of the sphere results in a nonzero lift, i.e., component of the hydrodynamics force in the direction normal to the stream wise direction. The detailed analysis of lift coefficient is presented in Ref. [23]. Here, we compare the relative magnitudes of drag and lift coefficients.

In Fig. 13, the ratio of drag to lift is shown as a function of *Y/H*. It can also be observed that all the C_D/C_L values are positive for case 1 as shown in Fig. 13(*a*), suggesting that the Janus sphere always has a lift directed toward the channel centerline for this configuration. The ratio is significantly higher at low values of Reynolds number and decreases with an increase in Reynolds number for both the cases. This suggests that at higher values of Reynolds number the lift becomes of the same order as that of drag.

For case 2, shown in Fig. 13(*b*), there is no definite trend visible for C_D/C_L. The change in sign is because of the change in direction of lift with the Janus positions in the channel. The ratio C_D/C_L do not follow a particular trend for case 2. Therefore, the variation of drag and lift coefficient with the sphere positions in the channel for case 2 is shown in Figs. 13(*d*) and 13(*e*). While drag decreases monotonically with *Y/H*, lift coefficient changes its sign with the Janus positions and with the particle Reynolds number. The nonmonotonic trend observed in drag to lift ratio can therefore be attributed to the change in lift.

5.5 Correlations for Drag Coefficient. Based on the drag coefficients obtained, correlations are proposed for the drag coefficient as a function of *Y/H* and Re_P. After a linear regression analysis, the correlations given by Eq. (6) obtained for case 1.

$$C_D = 13.4\,(Y/H)^{-0.73}\,Re_P^{-0.84} \tag{6}$$

The absolute average relative error (AARE) defined as, $\left(\text{AARE} = \frac{1}{n}\sum_{i=1}^{n}\frac{|\text{Predicted}-\text{CFD}|}{\text{CFD}} \times 100\right)(\%)$ is 19.3%. The correlation for case 2 is given by Eq. (7).

$$C_D = 22.69\,(Y/H)^{-0.50}\,Re_P^{-0.85} \tag{7}$$

The absolute average relative error (AARE) is 18.06%.

A parity plot for the comparison of CFD values and correlation values is shown in Fig. 14. The developed correlations are valid for all the positions of Janus particle ($0.1 \le Y/H \le 0.38$) and particle Reynolds numbers ($0.1 \le Re_P \le 50$) investigated. The R^2 value for drag coefficient correlations is 0.986 for case 1 and 0.984 for case 2, respectively.

Downloaded from http://asmedigitalcollection.asme.org/fluidsengineering/article-pdf/143/3/031302/6596983/fe_143_03_031302.pdf by Indian Institute Of Tech- Guwahati user on 03 August 2023

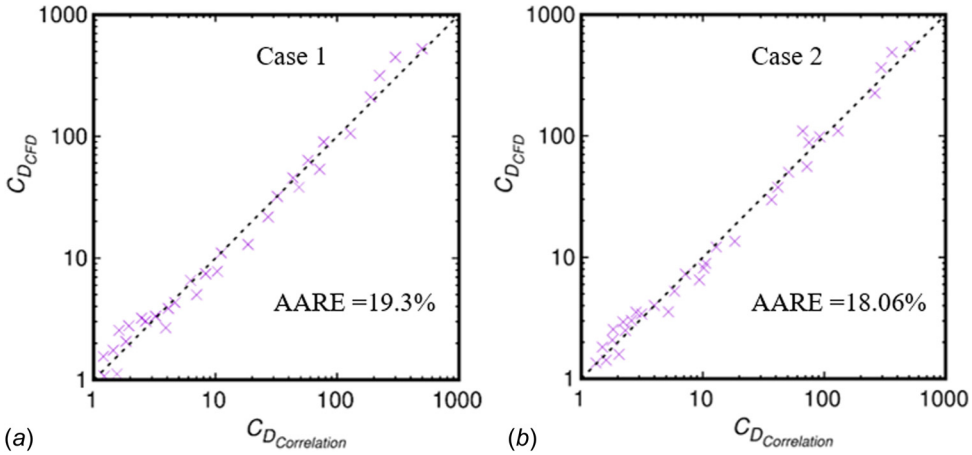

Fig. 14 The drag coefficient obtained from simulations is compared with the values obtained from proposed correlations based on linear regression. (*a*) For case 1 and (*b*) for case 2.

6 Conclusion

Three-dimensional CFD simulations are performed to calculate drag on a Janus sphere consisting of sticky and slippery hemispheres placed at different positions between the channel centerline and wall for $Re_P \leq 50$. The boundary between the two hemispheres of Janus particle is parallel to the channel midplane and two cases are considered: (1) slippery hemisphere facing the channel centerline and (2) sticky hemisphere facing the channel centerline.

The orientation of Janus sphere has a significant effect on the flow field surrounding the sphere. At higher value of Reynolds number, flow separation occurs on the no-slip hemisphere in case 2 and a vortex is observed. However, no flow separation occurs for case 1 for the values of Reynolds number investigated. Drag force on the Janus sphere lies in between those of stick and slip spheres and the drag is higher for case 2 than that for case 1. The drag coefficient is observed to decrease with an increase in particle Reynolds number and the dependence of drag coefficient on Reynolds number is observed to be the same $\left(C_D \sim Re_P^{-0.85}\right)$ for both the cases. The drag coefficient and the viscous and pressure contributions to the drag also decrease on moving the sphere closer to the channel wall. The dependence of drag coefficient on the dimensionless distance from the channel center is different for the two cases—$C_D \approx (Y/H)^{-0.73}$ for case 1 and $C_D \approx (Y/H)^{-0.50}$ for case 2. The magnitude of lift coefficient is negligible at low Re and becomes comparable to that of drag at higher Reynolds numbers.

A local drag coefficient, based on the fluid velocity approaching the center of the sphere, shows the effect of the channel wall on the drag. The local drag coefficient is observed to be almost independent of Y/H except near the wall where it increases sharply. The local drag coefficient also increases with an increase in particle Reynolds number.

Acknowledgment

M.D. thanks Ministry of Education, India, for providing the financial assistance in the form of PG scholarship.

Funding Data

- Ministry of Education, India (Funder ID: 10.13039/501100004541).

References

[1] Casagrande, C., Fabre, P., Veyssie, M., and Raphael, E., 1989, "Janus Beads: Realization and Behaviour at Water/Oil Interfaces," Europhys. Lett., **9**(3), pp. 251–255.

[2] Synytska, A., Khanum, R., Ionov, L., Cherif, C., and Bellmann, C., 2011, "Water-Repellent Textile Via Decorating Fibers With Amphiphilic Janus Particles," ACS Appl. Mater. Interfaces, **3**(4), pp. 1216–1220.

[3] Nisisako, T., Torii, T., Takahashi, T., and Takizawa, Y., 2006, "Synthesis of Monodisperse Bicolored Janus Particles With Electrical Anisotropy Using a Microfluidic Co-Flow System," Adv. Mater., **18**(9), pp. 1152–1156.

[4] Zhang, J., Zheng, X., Cui, H., and Silber-Li, Z., 2017, "The Self-Propulsion of the Spherical Pt–SiO2 Janus Micro-Motor," Micromachines, **8**(4), p. 123.

[5] Haney, B., Chen, D., Cai, L.-H., Weitz, D., and Ramakrishnan, S., 2019, "Millimeter–Size Pickering Emulsions Stabilized With Janus Microparticles," Langmuir, **35**(13), pp. 4693–4701.

[6] Costantini, R., Mollicone, J. P., and Battista, F., 2018, "Drag Reduction Induced by Superhydrophobic Surfaces in Turbulent Pipe Flow," Phys. Fluids, **30**(2), p. 025102.

[7] Dong, H., Cheng, M., Zhang, Y., Wei, H., and Shi, F., 2013, "Extraordinary Drag-Reducing Effect of a Superhydrophobic Coating on a Macroscopic Model Ship at High Speed," J. Mater. Chem. A, **1**(19), pp. 5886–5891.

[8] Gruncell, B., Sandham, N., and Mchale, G., 2013, "Simulations of Laminar Flow Past a Superhydrophobic Sphere With Drag Reduction and Separation Delay," Phys. Fluids, **25**(4), p. 043601.

[9] Vakarelski, I. U., Chan, D. Y. C., and Thoroddsen, S. T., 2014, "Leidenfrost Vapour Layer Moderation of the Drag Crisis and Trajectories of Superhydrophobic and Hydrophilic Spheres Falling in Water," Soft Matter, **10**(31), pp. 5662–5668.

[10] Safaei, S., Archereau, A., Hendy, C. S., and Willmott, R. G., 2019, "Molecular Dynamics Simulations of Janus Nanoparticles in a Fluid Flow," Soft Matter, **15**(33), pp. 6742–6752.

[11] Das, S., Garg, A., Campbell, A. I., Howse, J., Sen, A., Velegol, D., Golestanian, R., and Ebbens, S. J., 2015, "Boundaries Can Steer Active Janus Spheres," Nat. Commun., **6**(1), p. 8999.

[12] Uspal, W. E., Popescu, M. N., Tasinkevych, M., and Dietrich, S., 2018, "Shape-Dependent Guidance of Active Janus Particles by Chemically Patterned Surfaces," New J. Phys., **20**(1), p. 015013.

[13] Sun, Q., Klaseboer, E., Khoo, B. C., and Chan, D. Y., 2013, "Stokesian Dynamics of Pill Shaped Janus Particles With Stick and Slip Boundary Conditions," Phys. Rev. E, **87**, p. 43009.

[14] Shklyaev, S., Ivantsov, A., Díaz-Maldonado, M., and Córdova-Figueroa, U., 2013, "Dynamics of a Janus Drop in an External Flow," Phys. Fluids, **25**(8), p. 082105.

[15] Swan, J., and Khair, A., 2008, "On the Hydrodynamics of 'Slip–Stick' Spheres," J. Fluid Mech., **606**, pp. 115–132.

[16] Trofa, M., D'Avino, G., and Maffettone, P. L., 2019, "Numerical Simulations of a Stick-Slip Spherical Particle in Poiseuille Flow," Phys. Fluids, **31**(8), p. 083603.

[17] Dhiman, M., Ashutosh, S. A., Gupta, R., and Reddy, K. A., 2020, "Drag on Sticky and Janus (Slip-Stick) Spheres Confined in a Channel," ASME. J. Fluids Eng., **142**(7), p. 071303.

[18] Kempe, T., Lennartz, M., Schwarz, S., and Fröhlich, J., 2015, "Imposing the Free-Slip Condition With a Continuous Forcing Immersed Boundary Method," J. Comput. Phys., **282**, pp. 183–209.

[19] ANSYS, 2019, "ANSYS Academic Research Fluent, Release 19.2, Help System, Theory Guide," ANSYS Inc., Canonsburg, PA.

[20] Barth, T. J., and Jespersen, D., 1989, "The Design and Application of Upwind Schemes on Unstructured Meshes," AIAA Paper No. 1989-366.

[21] Issa, R. I., 1986, "Solution of Implicitly Discretized Fluid Flow Equations by Operator Splitting," J. Comput. Phys., **62**(1), pp. 40–65.

[22] Rhie, M. C., and Chow, W. L., 1983, "Numerical Study of the Turbulent Flow Past an Airfoil With Trailing Edge Separation," AIAA J., **21**(11), pp. 1525–1532.

[23] Dhiman, M., Gupta, R., and Reddy, K. A., 2020, "Lift Forces on Stick and Janus Spheres in a Channel," Theor. Comput. Fluid Dyn., ePub.

Downloaded from http://asmedigitalcollection.asme.org/fluidsengineering/article-pdf/143/3/031302/6596983/fe_143_03_031302.pdf by Indian Institute Of Tech- Guwahati user on 03 August 2023